Confined Doping on a Metallic Atomic Chain Structure

I. Barke, S. Polei, V. v. Oeynhausen, and K-H. Meiwes-Broer
Department of Physics, University of Rostock, D-18051 Rostock, Germany
(Received 25 May 2012; published 7 August 2012)

On Si(111)-(5 × 2)-Au it is shown that metallic sections of quantum wires between two doping adatoms establish a local electronic structure which is primarily defined by the section length. Such confined doping is a direct consequence of reduced dimensionality and is not observed in higher dimensions. Within a chain segment, the effect of a spatially independent charge-carrier concentration is superimposed by a Coulomb-like interaction due to the positively charged dopants. This offers a natural explanation for the relatively broad photoemission features and the complex appearance in scanning tunneling microscopy and spectroscopy images.

DOI: 10.1103/PhysRevLett.109.066801 PACS numbers: 73.20.At, 61.72.U−, 68.37.Ef, 73.21.Hb

Controlled doping of semiconductors is one of the most important technical achievements of the past century, which eventually led to the widespread availability of various electronic devices. Dopants adsorbed on metallic surfaces, on the other hand, are used as a versatile tool in fundamental science for precise band-structure engineering [1–4]. Such surface state doping is of delocalized nature since the impurities provide virtually free charge carriers that are not bound to the local adatom arrangement.

The situation becomes substantially different in one dimension, where the very dopants themselves can constrict the free distribution of charge carriers. As a result, only a limited region is affected by each dopant. In contrast to the well-known case of quantized electron states due to geometric confinement, the doping effect does not lead to energy and momentum quantization but primarily to an energetic shift of the local band structure with respect to the Fermi energy.

In this work, an experimental realization of such confined metallic doping is demonstrated. As a one-dimensional model system, atomic chains at semiconductor surfaces (for an overview, see [5–11]) are used which have proven to serve as an ideal basis for investigating exotic effects like fractional band filling [12], spin-orbit coupling of one-dimensional metallic bands [13,14], spontaneous magnetism [15], and Tomonaga-Luttinger liquid behavior [16]. Here, it is shown that atomic chains on Si(111)-(5 × 2)-Au naturally consist of metallic chain sections that are differently doped and separated by a single Si adatom. The sections exhibit a local electronic structure with well-defined carrier concentrations and energy offsets. Coupling across the adatoms is low. These are key ingredients toward precise tailoring of the local electronic structure via doping on the atomic level.

Previous studies revealed that the natural adatom concentration of Si(111)-(5 × 2)-Au (in the following referred to as 5 × 2) is crucial for the formation of the lowest-energy geometry [17,18]. On average, one Si atom per 5x8 unit cell results in optimum electron doping and in dimerization of essentially one of the three Au rows [18,19]. Interestingly, the Si adatoms do not form a regular pattern but an almost randomly distributed two-dimensional lattice fluid with a tendency of phase separation into 5 × 4 chains and empty sections [20–22]. Thus, the surface consists of adatom-free sections (AFS) of various lengths l_s, separated from each other by a single Si adatom. Perpendicular to the chains electron coupling is largely prevented by the Si honey-comb chain, a structural element shared by many related systems [5,23–25]. The interplay between electron injection into surface states and their interaction with the charged dopants are the scope of the following discussion.

For sample preparation, the Si(111) substrate (n-type) is degassed at 600 °C for about one hour and repeatedly flashed to 1250 °C. Gold is evaporated from an electron-beam evaporator at 650 °C sample temperature. A coverage of 0.6 ML Au leads to the Si(111)-(5 × 2)-Au reconstruction as shown in Fig. 1(a) [19]. Scanning tunneling microscopy (STM) and spectroscopy (STS) measurements are conducted at 78 K in a commercial low-temperature STM (Omicron Nanotechnology) with a modified preamplifier. Differential conductivity maps are recorded in open-loop mode (feedback switched off) using a lock-in detection method. The modulation amplitude $U_{\mathrm{mod,rms}} = 40$ mV (at ≈ 8 kHz) provides a good signal-to-noise ratio without significant peak broadening. The set point (SP) before switching off the feedback loop is $V_{\mathrm{SP}} = -1.5$ V and $I_{\mathrm{SP}} = -0.3$ nA for all spectra. A linear z-ramp (0.1 nm/V) during spectroscopy partially compensates for the exponentially increasing transmission as a function of applied sample bias [26].

Figure 1 displays the topography and two simultaneously recorded dI/dV maps of the 5 × 2 surface. The adatom locations are extracted from Fig. 1(a) and indicated by white circles in the lower two panels. Pronounced variations of the local density of states (LDOS) are evident from Fig. 1(b), where long AFS appear bright while the signal is low at the equivalent atomic location within short

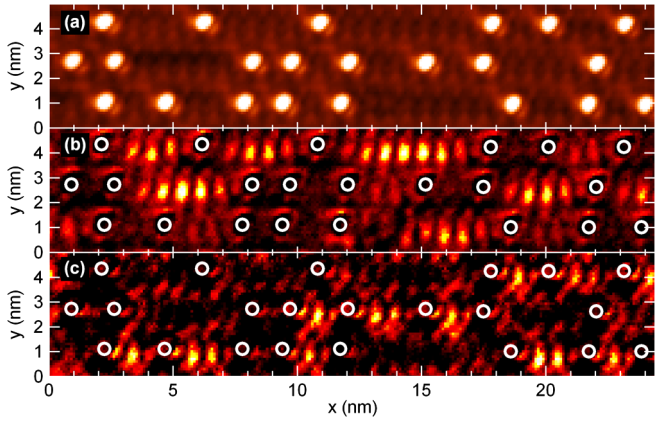

FIG. 1 (color online). (a) Topographic STM image of 5×2 recorded simultaneously with the spectroscopic data in (b) and (c). The chains are aligned horizontally. (b) dI/dV map at $V_{\text{sample}} = -1.03$ V. Long adatom-free sections (AFS) appear bright indicating high density of states. (c) dI/dV map at $V_{\text{sample}} = -1.19$ V. Long AFS appear dark indicating low density of states. Different appearance of long and short AFS within each map is caused by an energetic shift of the local electronic structure (see Fig. 2).

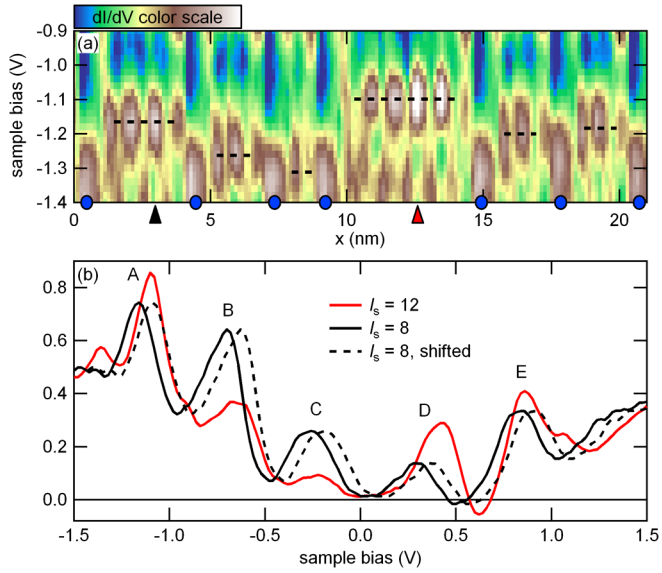

FIG. 2 (color online). (a) STS spectra as a function of location along the chains. Horizontal dashed lines correspond to the positions of peak A in the dI/dV curves [cf. Fig. 2(b)]. The locations of the adatoms are marked by blue circles. (b) STS spectra for an extended energy range measured at the locations indicated by triangles in (a). The length of the corresponding AFS is $l_s = 12$ ($l_s = 8$) for the red (black) curve. The dashed spectrum represents the $l_s = 8$ case but is shifted horizontally by 72 mV for better comparison to the red curve. The five pronounced peaks are labeled A-E. They essentially correspond to band edges, which shift relative to the Fermi level due to a change in the band filling. That, in turn, is caused by charge transfer from the two dopant atoms terminating an adatom-free section.

AFS. At slightly lower voltages, the situation reverses and the short AFS appear bright [Fig. 1(c)]. A movie showing STS data for a continuous energy range can be found in the Supplemental Material [27]. The periodicity seen between the adatoms corresponds to the twofold superstructure of 5×2.

A systematic study of the electronic structure for a restricted energy range is illustrated in Fig. 2(a). It shows the dI/dV signal as a function of energy and location along the Au double chains in the occupied spectral region. Two main features are visible within this energy interval, one at about 1.35 eV located at the adatom positions [blue circles in Fig. 2(a)] and others located between the adatoms, inside the AFS [dashed lines in Fig. 2(a)]. The latter occur at higher energy between -1.3 and -1.1 eV and are referred to as state A in the following.

Earlier STS reports have attributed energy shifts of spectral features on 5×2 to the presence of Si adatoms [28,29]. Indeed, state A changes its energy depending on the local adatom environment. Interestingly, the energy position within an AFS (indicated by dashed lines) only shows a weak dependence on the distance to the next adatom. In contrast it varies significantly among different sections across the adatoms. This situation is very different from the well investigated effect of single dopants in semiconductors [30–35], where the impurities give rise to a local band bending with an almost isotropic Coulomb shift which is approximately inversely proportional to the adatom distance. In fact, it will be shown below that on 5×2 such a Coulomb potential is efficiently screened on the AFS since the reconstruction is metallic between the adatoms [28,29]. A comparison of STS curves in an extended energy range is shown in Fig. 2(b) for AFS of different lengths l_s given in units of a bulk Si-Si distance along the chain $a_{\text{Si}} = 3.84$ Å. Displacing the curve for $l_s = 8$ (black) horizontally by 72 mV results in a good match of all peak positions A-E of the curve for $l_s = 12$ (dashed vs. red). Thus, the entire spectrum experiences a rigid shift which is not restricted to particular features.

The STS spectra in Fig. 2(b) are now compared to photoemission data reported in the literature. All occupied features can be assigned to edges of individual surface bands. State A corresponds to the bottom of the band labeled S3, S4, and 2 in Refs. [18,36,37], respectively. Accordingly, states B and C can be identified being caused by the respective band edges of $1'$ and $1''$ in Ref. [18]. Unoccupied states are not accessible by photoemission, but state D is consistent to DFT calculations [18], and state E has been observed in inverse photoemission [38]. Further confidence in the STS data quality is provided by analyzing the spatial occurence of the states. Maximum charge density of state A, for instance, is detected on the Au double row in the dimer regions [39] consistent to first-principles calculations [18].

In order to investigate the origin of the rigid shift, the electronic structure of different AFS is studied as a function of the section lengths l_s. In Fig. 3(a) dI/dV spectra recorded in the center of each AFS are shown for various l_s. Analyzing the peak position of state A, a systematic downshift ΔE is evident for decreasing l_s [inset of Fig. 3(b)]. It is attributed to electron injection into surface bands by the donor adatoms, resulting in a rigid energy shift of the bands relative to the Fermi level within each AFS. Tip-induced band bending is excluded by varying the set point conditions and by the voltage independence of the shift (see also [40]). Interchain coupling is low since no significant correlation of the peak position between neighboring chains could be found. Along the chains weak coupling across the adatoms is measurable for the shortest sections reflected by slight variations of the energetic shift among AFS of same length [cf. Fig. 2(a)]. This minor shift is attributed to a Coulomb-like effect (see below). Hence, the surface primarily consists of an arrangement of differently doped sections with well-defined local surface states, separated by single Si adatoms. The magnitude of ΔE is consistent with results from photoemission experiments for different average adatom concentrations [36]. The shift depends on the one-dimensional electron concentration which is given by the number of doping electrons n_A per Si adatom divided by l_s. From density functional calculations $n_A = 2$ has been found [18], limiting the maximum doping concentration to $\approx 0.13\ \mathrm{nm}^{-1}$ for the shortest AFS ($l_s = 4$) [41]. Plotting the energy shift as a function of inverse length, a linear relation with a slope $m = -0.27$ eV nm is obtained that reflects successive band filling induced by the dopants [Fig. 3(b)].

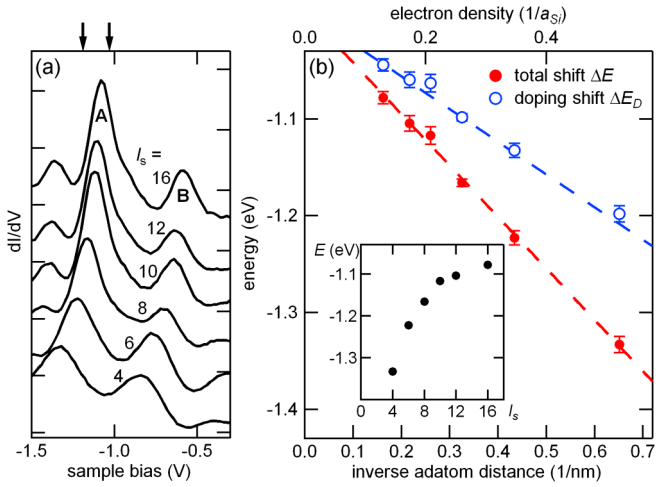

FIG. 3 (color online). (a) dI/dV spectra at the center of AFS, each of them averaged over several sections of same lengths l_s (given in units of a bulk Si-Si distance along the chain a_{Si}). Curves are offset vertically for clarity. Arrows indicate voltages for the dI/dV maps in Figs. 1(b) and 1(c). The continuous downward shift for decreasing l_s is caused by an increase in local carrier concentration and the interaction with the charged dopands. (b) Peak position as a function of inverse adatom distance (bottom axis) and electron concentration (top axis) within the AFS. Solid circles: raw data; open circles: after correction for the Coulomb interaction with neighboring adatoms. The error bars reflect the standard deviation of results obtained from the different AFS. Inset: Peak position of state A obtained from a Gaussian fit from (a).

Part of the shift ΔE, however, is caused by electronic coupling to both neighboring adatoms: each donor adatom affects its local electronic environment via Coulomb interaction of the ion core, similar to the case of bulk dopants (see, e.g., [30–35]). Although relatively weak, the Coulomb-effect on the surface states can be measured on long AFS as a function of location within the section. In Fig. 4, the energy position of state A is shown together with a fit to the sum of two Coulomb-like potentials of the form $\phi(x) = \phi_0 - \sum_i c/|x - x_i|$, where the x_i are the locations of the adatoms and c is a constant depending on the material properties.

The fit yields $c = 0.05$ eV nm and is, therefore, a factor ≈ 50 smaller compared to a doubly charged ion in vacuum. This is a strong indication for efficient screening by the metallic electrons in the AFS. The downward shift ΔE_C of the surface bands in vicinity of the adatoms confirms their n-type doping effect and is consistent to earlier reports [29,36]. For this analysis, an area with low adatom concentration in the vicinity of the AFS has been chosen to avoid electrostatic interaction with several adatoms. It is worth noting that the Coulomb-like shift ΔE_C induced by adatoms of neighboring chains (i.e., in perpendicular direction) is significantly weaker, such that the interaction has an anisotropic character. The detailed mechanism for this anisotropy is left as a topic for future investigations. The total energy shift induced by the adatoms can now be assigned to two contributions, the doping-induced shift ΔE_D which corresponds to a population of states by adatom electrons, and a Coulomb-like interaction ΔE_C due to

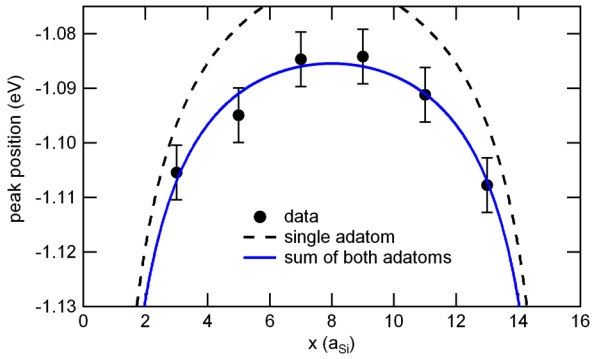

FIG. 4 (color online). Measured energy position (circles) of state A [see Fig. 2(b)] on an AFS ($l_s = 16$) as a function of location along the chain. Blue solid curve: fit of a Coulomb-like potential induced by both adatoms. The dashed curves represent the two components of the individual adatoms located at $x = 0$ and $x = 16$, respectively.

the charged impurities. Extraction of ΔE_D from the measured total shift ΔE [full circles in Fig. 3(b)] yields: $\Delta E_D = \Delta E - \Delta E_C$, $\Delta E_C = 2c/(\frac{l_s}{2})$. The component ΔE_D is plotted in Fig. 3(b) (open circles) resulting in a slope $m_D = -0.16$ eV nm. Interestingly, the energy shift can be transformed to an absolute value of the LDOS at the Fermi level. Within the AFS, such an estimation yields $\mathrm{LDOS} = \frac{dN/dE}{L} = \frac{n_A}{|m_D| a_{\mathrm{Si}}} \approx 3.3(\mathrm{eV\,\AA})^{-1}$. At present this first estimate for the total LDOS on the double Au row on 5×2 cannot be compared to other experimental data since it is not accessible by conventional STS.

In conclusion, adatoms on Si(111)5×2-Au act as dopants for the local electronic environment. A constant doping level is established within each chain segment between the adatoms, apart from a small Coulomb shift due to interaction with the positively charged dopant cores. The local electronic structure on segments of various lengths mainly differs by a rigid energetic shift depending only weakly on the distance to the next adatom. This results in well-separated, differently doped sections which are decoupled from each other by a single Si impurity. The interplay between confined doping and a Coulomb-like interaction with the adatoms results in strongly energy-dependent LDOS contrast in atomically resolved STS measurements. Nonlocal methods average over many such sections which offers a simple and natural explanation for the rather broad spectral features observed in photoelectron spectroscopy [20,36]. In conjunction with atom manipulation techniques [42], the present results open new routes for quantitative and local control of electron states in metallic nanostructures on the atomic scale, particularly if other atomic species are involved [43,44].

We thank H. Pfnür and Th. Fennel for fruitful discussions. Funding by the federal state Mecklenburg-Vorpommern within the project Nano4Hydrogen is gratefully acknowledged.

[1] S. Å. Lindgren and L. Walldén, Solid State Commun. **28**, 283 (1978).
[2] S. Å. Lindgren and L. Walldén, Solid State Commun. **34**, 671 (1980).
[3] J. N. Crain, M. C. Gallagher, J. L. McChesney, M. Bissen, and F. J. Himpsel, Phys. Rev. B **72**, 045312 (2005).
[4] H. Morikawa, C. C. Hwang, and H. W. Yeom, Phys. Rev. B **81**, 075401 (2010).
[5] J. N. Crain, J. L. McChesney, F. Zheng, M. C. Gallagher, P. C. Snijders, M. Bissen, C. Gundelach, S. C. Erwin, and F. J. Himpsel, Phys. Rev. B **69**, 125401 (2004).
[6] I. Barke, R. Bennewitz, J. N. Crain, S. C. Erwin, A. Kirakosian, J. L. McChesney, and F. J. Himpsel, Solid State Commun. **142**, 617 (2007).
[7] I. Barke, T. K. Rügheimer, F. Zheng, and F. J. Himpsel, Appl. Surf. Sci. **254**, 4 (2007).
[8] N. Oncel, J. Phys. Condens. Matter **20**, 393001 (2008).
[9] J. Schaefer *et al.*, New J. Phys. **11**, 125011 (2009).
[10] P. C. Snijders and H. H. Weitering, Rev. Mod. Phys. **82**, 307 (2010).
[11] S. Hasegawa, J. Phys. Condens. Matter **22**, 084026 (2010).
[12] J. N. Crain, A. Kirakosian, K. N. Altmann, C. Bromberger, S. C. Erwin, J. L. McChesney, J.-L. Lin, and F. J. Himpsel, Phys. Rev. Lett. **90**, 176805 (2003).
[13] D. Sánchez-Portal, S. Riikonen, and R. M. Martin, Phys. Rev. Lett. **93**, 146803 (2004).
[14] I. Barke, F. Zheng, T. K. Rügheimer, and F. J. Himpsel, Phys. Rev. Lett. **97**, 226405 (2006).
[15] S. C. Erwin and F. J. Himpsel, Nature Commun. **1**, 58 (2010).
[16] C. Blumenstein, J. Schäfer, S. Mietke, S. Meyer, A. Dollinger, M. Lochner, X. Y. Cui, L. Patthey, R. Matzdorf, and R. Claessen, Nature Phys. **7**, 776 (2011).
[17] S. C. Erwin, Phys. Rev. Lett. **91**, 206101 (2003).
[18] S. C. Erwin, I. Barke, and F. J. Himpsel, Phys. Rev. B **80**, 155409 (2009).
[19] I. Barke, F. Zheng, S. Bockenhauer, K. Sell, V. v. Oeynhausen, K. H. Meiwes-Broer, S. C. Erwin, and F. J. Himpsel, Phys. Rev. B **79**, 155301 (2009).
[20] J. L. McChesney, J. N. Crain, V. Pérez-Dieste, F. Zheng, M. C. Gallagher, M. Bissen, C. Gundelach, and F. J. Himpsel, Phys. Rev. B **70**, 195430 (2004).
[21] A. Kirakosian, J. N. Crain, J.-L. Lin, J. L. McChesney, D. Y. Petrovykh, F. J. Himpsel, and R. Bennewitz, Surf. Sci. **532–535**, 928 (2003).
[22] A. Kirakosian, R. Bennewitz, F. J. Himpsel, and L. W. Bruch, Phys. Rev. B **67**, 205412 (2003).
[23] S. C. Erwin and H. H. Weitering, Phys. Rev. Lett. **81**, 2296 (1998).
[24] S. Riikonen and D. Sánchez-Portal, Phys. Rev. B **77**, 165418 (2008).
[25] M. Krawiec, Phys. Rev. B **81**, 115436 (2010).
[26] R. M. Feenstra, Phys. Rev. B **50**, 4561 (1994).
[27] See Supplemental Material at http://link.aps.org/supplemental/10.1103/PhysRevLett.109.066801 for a movie showing the varying contrast on the AFS.
[28] H. S. Yoon, S. J. Park, J. E. Lee, C. N. Whang, and I. W. Lyo, Phys. Rev. Lett. **92**, 096801 (2004).
[29] H. S. Yoon, J. E. Lee, S. J. Park, I. W. Lyo, and M. H. Kang, Phys. Rev. B **72**, 155443 (2005).
[30] M. B. Johnson, O. Albrektsen, R. M. Feenstra, and H. W. M. Salemink, Appl. Phys. Lett. **63**, 2923 (1993).
[31] J. F. Zheng, X. Liu, N. Newman, E. R. Weber, D. F. Ogletree, and M. Salmeron, Phys. Rev. Lett. **72**, 1490 (1994).
[32] T. Trappmann, C. Sürgers, and H. von Löhneysen, Europhys. Lett. **38**, 177 (1997).
[33] C. Sürgers, M. Schöck, T. Trappmann, and H. v. Löhneysen, Appl. Surf. Sci. **212–213**, 105 (2003).
[34] C. Wittneven, R. Dombrowski, M. Morgenstern, and R. Wiesendanger, Phys. Rev. Lett. **81**, 5616 (1998).
[35] H. Zheng, J. Kröger, and R. Berndt, Phys. Rev. Lett. **108**, 076801 (2012).
[36] W. H. Choi, P. G. Kang, K. D. Ryang, and H. W. Yeom, Phys. Rev. Lett. **100**, 126801 (2008).
[37] I. Matsuda, M. Hengsberger, F. Baumberger, T. Greber, H. W. Yeom, and J. Osterwalder, Phys. Rev. B **68**, 195319 (2003).
[38] I. G. Hill and A. B. McLean, Appl. Surf. Sci. **123–124**, 371 (1998).

[39] The exact location of the LDOS maximum can be determined by comparison of Fig. 2b and c to the structural model in Ref. [18].

[40] K. Sell, I. Barke, S. Polei, C. Schumann, V. v. Oeynhausen, and K.-H. Meiwes-Broer, Phys. Status Solidi B **247**, 1087 (2010).

[41] $l_s = 2$ is only rarely observed and thus not considered in this work [21,22].

[42] R. Bennewitz, J. N. Crain, A. Kirakosian, J.-L. Lin, J. L. McChesney, D. Y. Petrovykh, and F. J. Himpsel, Nanotechnology **13**, 499 (2002).

[43] A. Stępniak, P. Nita, M. Krawiec, and M. Jalachowski, Phys. Rev. B **80**, 125430 (2009).

[44] A. Stępniak, M. Krawiec, G. Zawadzki, and M. Jałochowski, J. Phys. Condens. Matter **24**, 095002 (2012).